Bulletin of the *Transilvania* University of Brasov
Series II: Forestry • Wood Industry • Agricultural Food Engineering • Vol. 17(66) No. 2 – 2024
https://doi.org/10.31926/but.fwiafe.2024.17.66.2.5

# A 30-YEAR ANALYSIS OF FOREST COVER AND LAND SURFACE TEMPERATURE IN ATTAPEU PROVINCE, LAO PDR

**Vu T. PHUONG[1] Bounheuang YACHONGTOU[2]**
**Ioshpa R. ALEXSANDER[3] Bui B. THIEN[3]**

***Abstract:*** *Changing forest areas can have a complex range of impacts on ground temperatures, from increasing temperatures due to loss of shade to creating drier and hotter local climate environments. This study aims to identify spatiotemporal changes in forest cover and retrieve land surface temperature (LST) using thermal infrared sensor (TIRS) data in Attapeu province, Lao PDR from 1994 to 2024. Geographic information system (GIS) techniques were employed to extract spatiotemporal changes in land use and land cover (LULC) and Normalized Difference Vegetation Index (NDVI). The analysis of LULC change revealed a notable decrease of 18.43% in dense forest areas, accompanied by an increase of 7.87% in sparse forest and 11.35% in cropland, indicating a transition from dense forest to sparse forest and cropland for the study area. The analysis of LST utilizing TIRS revealed a consistent negative correlation with NDVI. The coefficient of determination ($R^2$) indicated values of 0.5896 in 1994, 0.5691 in 2009, and 0.4344 in 2024. By correlating remotely-sensed thermal data with in situ observations, this research delineated the prolonged alterations in LST due to fluctuations in forest cover. The urgency of enacting policies is underscored to mitigate the ongoing loss of forest cover. These findings emphasize the need for immediate policy actions, such as enhanced forest conservation and reforestation programs, to mitigate rising temperatures and ensure ecological sustainability in Attapeu province. The insights garnered from this investigation hold significant implications for the conservation endeavors aimed at preserving the forests of Attapeu province.*

***Key words:*** *land surface temperature, vegetation index, remote sensing, maximum likelihood classifier.*

[1] Innovation Startup Support Center, Hong Duc University, Thanh Hoa, Vietnam;
[2] Faculty of Social Sciences, National University of Laos, Vientiane, Laos;
[3] Institute of Earth Sciences, Southern Federal University, Rostov-on-Don, Russia;
Correspondence: Bui B. Thien; email: buibaothienha@gmail.com.

## 1. Introduction

Forest resources encompass both biotic and abiotic elements. These resources satisfy human needs and contribute to national economies [1, 4, 5, 12]. Forests provide ecosystem goods and services, including timber, wildlife, water, soil, and recreational opportunities [22, 38, 51]. Forest composition determines the diversity of products that the forest can offer. Forests cover approximately 31% of the global land area, but their distribution is uneven worldwide [10]. Nearly half of the forest area remains relatively intact, with over one-third classified as primary forest [16]. However, deforestation and forest degradation continue at alarming rates, leading to biodiversity loss [38, 42, 43].

Currently, deforestation is exacerbating worldwide, significantly impacting land surface temperatures (LST) [9, 13, 14, 19]. For example, in the Amazon and Southeast Asia, studies have shown that deforestation contributes to rising temperatures and disrupted rainfall patterns [21, 59]. This process substantially reduces evaporation and slightly increases light reflection, consequently contributing to global climate warming [22, 23]. Particularly, limiting forest clearance plays a crucial role in preserving the dense ecological network of forests and maintaining surface temperatures within manageable limits [23, 27]. Internationally, deforestation is recognized as a leading cause of global warming and a significant factor in biodiversity loss. Studies such as those by Wang and Azam [58] have demonstrated how deforestation leads to increased greenhouse gas emissions, significantly altering regional and global climate systems. The loss of forests leads to the extinction of thousands of animal and plant species [2, 20]. Failure to curb deforestation could push global warming to an irreversible scenario, as evidenced by numerous scientific studies [30, 43, 58]. LST is a reliable indicator of the forest's impact on temperature and can therefore be used to assess the effects of deforestation [25, 34, 42]. Deforestation can directly contribute to global warming through light reflection and indirectly through increased greenhouse gases. This could significantly alter ecosystem structure, signaling a future where LST will continue to rise [28, 29, 50].

Remote sensing and geographic information systems (GIS) play a crucial role in studying these relationships and assessing the impact of forest change on local climate [24, 55, 56, 57, 61]. Remote sensing techniques combined with GIS allow researchers to estimate deforestation rates, analyze land use practices, assess biodiversity, and more [38, 40, 52]. These tools provide valuable insights into the impact of forest cover changes on LST, especially in tropical and temperate regions. This study distinguishes itself by focusing on Attapeu province, employing advanced LST retrieval techniques and integrating NDVI analysis to offer localized insights into forest dynamics over a 30-year period. The integration of satellite imagery with GIS has proven effective in estimating and analyzing changes in land use and land cover (LULC) types [9, 11, 30, 53]. Furthermore, combining remote sensing data with ground measurements allows for precise LST calculations using advanced algorithms. The Normalized

Difference Vegetation Index (NDVI) emerges as a crucial indicator for assessing changes in LULC, providing insights into vegetation cover quantity and vitality, closely linked to LST [2, 3, 14]. Previous studies have used analyses of changes in LULC and NDVI to identify areas most susceptible to increased LST, providing valuable insights into regional vulnerability [2, 39, 55]. This comprehensive approach that combines advanced satellite technology with GIS and ground measurements enhances our understanding of the dynamics of LST and its relationship with various environmental factors [14, 55].

Several studies have delved into understanding land cover dynamics and their consequential impact on ecosystem services and regional climate. This paper delves into the intricate interplay between forest cover, LST, and Normalized Difference Vegetation Index (NDVI) within Attapeu province, Lao PDR. Utilizing remote sensing and GIS techniques, the analysis spans from 1994 to 2024. The preliminary exploration scrutinizes the influence of alterations in forest cover on LST and NDVI dynamics within the study area. Furthermore, our research delves into the synergy between forest cover and sophisticated LST retrieval algorithms, such as the Brightness Temperature (BT) method, emissivity-corrected LST estimation, and regression analysis utilizing NDVI, highlighting the spatial and temporal vicissitudes within this ecosystem.

This study pioneers the assessment of LST variations within Attapeu province, Lao PDR, throughout a three-decade time span. By employing remote sensing and GIS methodologies, it probes into the repercussions of forest cover alterations, human interventions, and climate variations on LST patterns. It addresses pertinent gaps in understanding environmental dynamics in the study locale and contributes insights to global issues concerning forced migrations, ecosystem resilience, deforestation, and the exacerbation of climate change in developing nations.

## 2. Materials and Methods

### 2.1. Study Area

Attapeu is a province located in the southeast tip of Lao PDR, between latitude 14°17'31.65"N to 15°19'52.74"N and longitude 106°10'6.58"E to 107°35'11.71"E, with a total area of 10,320 $km^2$ (Figure 1) [36]. It is best known for the Bolaven Plateau, sharing borders with Sekong province, Lao PDR in the North, Champasack province, Lao PDR in the West, Vietnam in the East, and Cambodia in the South. The terrain of this province mainly consists of mountains crossed by, river valleys, thus creating conditions for diverse ecological development. The province's landscape includes dense forests, rivers and plains, against the backdrop of mountain ranges such as Phou Saphong and Phou Luang. Attapeu province contains many precious natural heritage objects of Lao PDR, such as Xe Pian National Park and Dong Ampham National Park. The forest ecosystems are predominantly tropical and include a mix of evergreen and deciduous forests. Key tree species include dipterocarps, teak, and various hardwoods, while the forests also provide habitats for rare wildlife such as Asian elephants, gibbons, and hornbills. In terms of climate, Attapeu province has a humid tropical climate, with the rainy season

lasting from May to October and the dry season from November to April. Rainfall during the rainy season can be quite heavy, especially in July and August, while the average annual temperature ranges from 22 to 28°C.

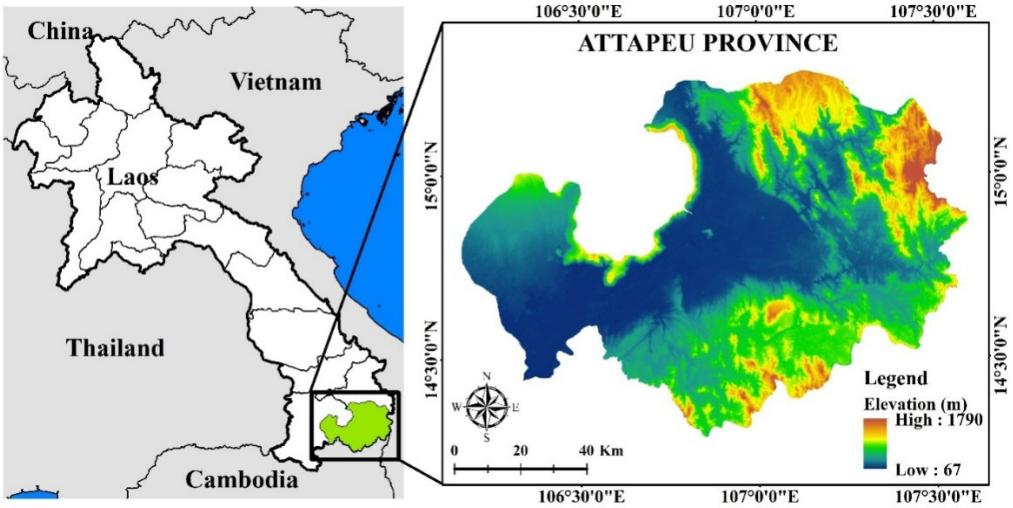


Fig. 1. *Map showing the study area in Attapeu province, Lao PDR*

**2.2.Data Collection and Pre-Processing**

This research employs multispectral data from Landsat 5 Thematic Mapper (TM) and Landsat 8 Operational Land Imager (OLI) made available by the United States Geological Survey (USGS) through the Earth Explorer service (https://earthexplorer.usgs.gov/) for the years 1994, 2009, and 2024 to examine the temporal dynamics of forest cover and LST in Attapeu province, Lao PDR (Table 1). Images were selected based on date (collected in January, during the summer) and based on them having no cloud cover. While Table 1 indicates that some scenes have up to 53% cloud cover, this value refers to the total cloud cover across the entire satellite scene. For this study, only the cloud-free portions of the imagery corresponding to the study area were extracted and used, ensuring that the analysis of forest cover and LST was not affected by cloud interference. The analysis utilized the blue, green, red, and near-infrared (NIR) spectral bands of Landsat 5 TM and Landsat 8 OLI, in order to delineate changes in forest cover. Additionally, thermal infrared (TIR) band 6 for Landsat 5 TM, along with TIR bands 10 and 11 for Landsat 8 OLI, were used in the present study for LST retrieval. These thermal bands measure radiance emitted from the Earth's surface in the thermal infrared spectrum. The data from these bands are converted into brightness temperature using calibration constants K1 and K2, which are sensor-specific values provided in Landsat metadata file (Table 1).

The LULC model underwent classification into four distinct categories: dense forests, sparse forests, non-forests, cropland, and water bodies. This classification was informed by both field survey data and detailed imagery from Google Earth Pro. To assess the accuracy of the LULC classification map, 300

sampling points were utilized for each respective year. For the years 1994 and 2009, sample points were sourced from Google Earth Pro imagery, while field surveys were carried out in January 2024for the images corresponding to that year. The survey covered key regions across Attapeu province, representing diverse LULC classes such as dense forests, sparse forests, croplands, and water bodies, with a total of 300 ground truth points collected using a stratified random sampling method. Figure 2 shows the spatial distribution of these sample points across the province.

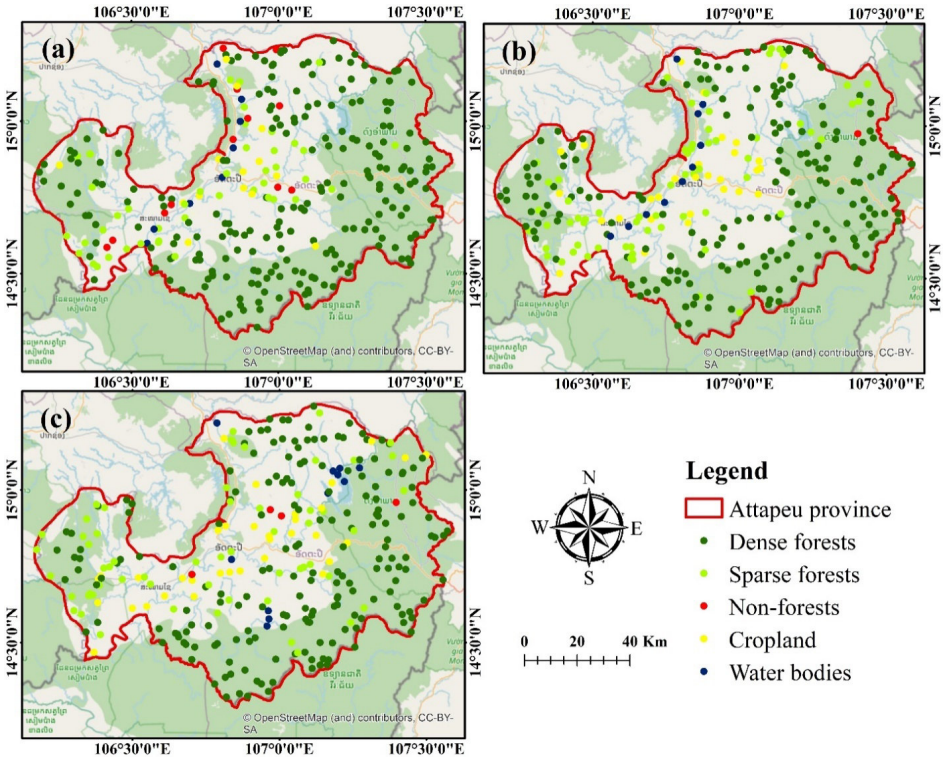


Fig. 2. *Geographic distribution of point samples*

### 2.3. Preprocessing and Image Classification

Satellite imagery spanning three years (1994, 2009, and 2024) underwent initial preprocessing steps. This involved rectifying radiometric, atmospheric, and geometric discrepancies present in the raw image data to ensure alignment with the coordinate system of the acquired images and the corresponding shapefile used for data processing. To enhance visualization and analysis, we consolidated the data into a single raster dataset with a predefined band composition [26]. Specifically, we combined bands 1 - 4 from Landsat 5 TM and the computed NDVI values, along with bands 2 - 5 from Landsat 8 OLI and their respective NDVI values [43]. These bands were chosen for their suitability in detecting changes in forest cover and facilitating true and false color representations, aiding in accuracy assessment and sample training.

Table 1

*General information about Landsat TM, OLI, and TIRS satellite data acquired in 1994, 2009, and 2024*

| Satellite | Acquisition data | Band used | Landsat Scene ID | Path/row | Cloud cover [%] | Thermal constants | | Sun Elevation [in degree] | Sun Azimuth [in degree] |
|---|---|---|---|---|---|---|---|---|---|
| | | | | | | K1 | K2 | | |
| Landsat 5 (TM/TIRS) | 30/01/1994 | 1, 2, 3, 4, & 6 | LT51250491994030BKT00 | 125/049 | 53.00 | 607.76 | 1260.56 | 39.95 | 130.71 |
| | | | LT51250501994030BKT00 | 125/050 | 1.00 | | | 40.73 | 129.59 |
| Landsat 5 (TM/TIRS) | 23/01/2009 | 1, 2, 3, 4, & 6 | LT51250492009023BKT01 | 125/049 | 12.00 | 607.76 | 1260.56 | 43.23 | 137.93 |
| | | | LT51250502009023BKT01 | 125/050 | 0.00 | | | 44.14 | 136.78 |
| Landsat 8 (OLI/TIRS) | 17/01/2024 | 2, 3, 4, 5, & 10 | LC81250502024017LGN00 | 125/050 | 1.74 | 774.89 | 1321.08 | 45.71 | 142.26 |

Subsequently, the relevant sections depicting the study area were extracted from the composite images of 1994, 2009, and 2024. For LULC classification, we employed a rule-based supervised classification method utilizing the maximum likelihood classifier algorithm [44, 47, 54]. This approach allows for the manual selection of pixels representing specific classes, ensuring consistency in category definitions and clear delineation of class boundaries based on natural and anthropogenic features within the study area [46, 54]. While the use of Google Earth Pro provides valuable historical context, the lack of direct field validation for 1994 and 2009 limits the precision of these classifications. The classification included five distinct classes: dense forests, sparse forests, non-forests, cropland, and water bodies. The classification methodology is detailed in Figure 3.

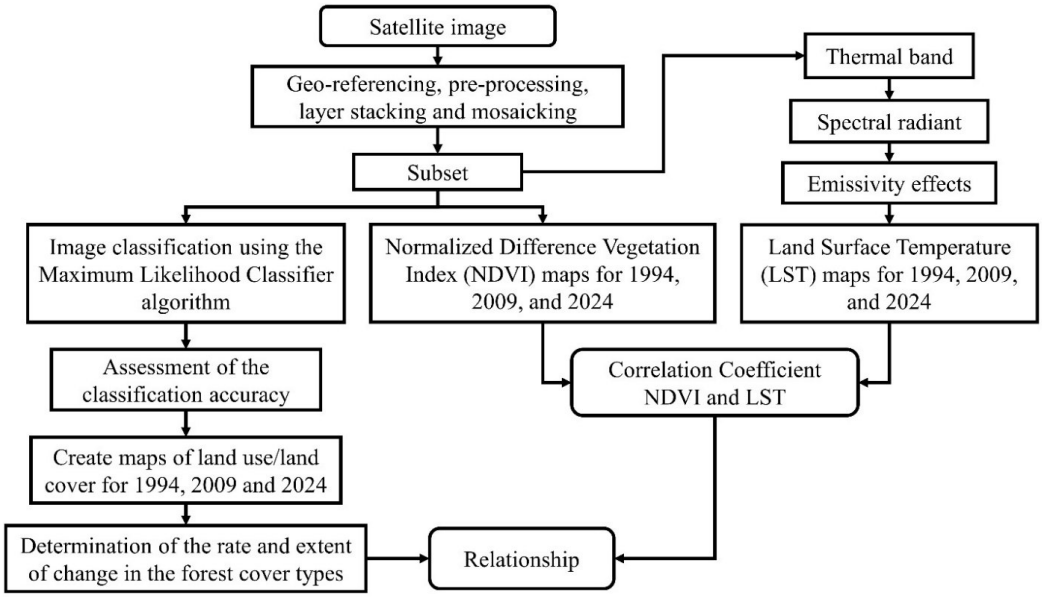


Fig. 3. *Overall process of forest cover change technique*

**2.4. Classification Accuracy Assessment**

The assessment of image classification accuracy was conducted on each of the three classified images utilizing a reference dataset comprising 300 points. For accuracy evaluation, the validation datasets were randomly partitioned to generate a confusion matrix, allowing the assessment of overall accuracy and kappa coefficient according to Equations (1) and (2), respectively [8, 29, 56].

$$\mathrm{OA} = \frac{\text{Number of sampling classes classified correctly}}{\text{Number of reference sampling classes}} \cdot 100 \quad (1)$$

$$\text{Kappa coefficient (K)} = \frac{\text{Po - Pe}}{1 - \text{Pe}} \quad (2)$$

where:

Po is the proportion of pixels classified correctly;

Pe - the proportion of pixels classified correctly expected by chance.

**2.5.Calculation of NDVI and LST**

NDVI serves as a metric for assessing the growth and vitality of vegetation within a given area, derived from the spectral reflectance properties of the surface [2, 14, 39]. In this study, the NDVI values are determined using the red and near-infrared (NIR) bands of Landsat imagery [52, 55]. Specifically, for Landsat TM, bands 3 and 4 are utilized, while for Landsat OLI, bands 4 and 5 are employed in the computation of NDVI. These bands are processed through stacking and layer division procedures within the study region, and Equation (3) is applied to calculate the NDVI values.

$$\text{NDVI} = \frac{\text{NIR - RED}}{\text{NIR} + \text{RED}} \quad (3)$$

The Landsat 5 TM thermal infrared band 6 (10.4–12.5 μm) and the Landsat 8 OLI thermal infrared band 10 (10.6–11.19 μm) data were used to obtain LST in degrees Celsius [30, 37, 41].

The Equations (4) and (5) were used to convert the digital number (DN) values of bands 6 and 10, respectively, into spectral irradiance at the sensor [24].

$$L_\lambda = \left( \frac{L_{max\lambda} - L_{min\lambda}}{QCal_{max} - QCal_{min}} \right) \cdot \left( QCal - QCal_{min} \right) + L_{min\lambda} \quad (4)$$

where:

$L_\lambda$ represents the sensor radiance:

$L_{max\lambda}$ – the maximum radiance of band 6;

$L_{min\lambda}$ – the minimum radiance of band 6

QCal – the quantized calibrated pixel value in DN;

$QCal_{max}$ – the maximum quantized calibrated pixel value in DN;

$QCal_{min}$ – the minimum quantized calibrated pixel value in DN.

$$L_\lambda = M_L \cdot QCal + A_L \quad (5)$$

where:

$M_L$ is the radiance multiplicative scaling factor;

$A_L$ – the radiance additive scaling factor for band 10.

Brightness Temperature (Tb) was obtained from Equation (6) [55].

$$Tb = \frac{K_2}{\ln\left( \frac{K_1}{L_\lambda} + 1 \right)} - 273.15 \quad (6)$$

where $K_1$ and $K_2$ are the calibration constants of thermal bands (Table 1).

Then, Equation (7) was used to determine the LST calculated in degrees Celsius [55].

$$LST_{(°C)} = \frac{Tb}{1 + \frac{\lambda \cdot Tb}{\rho}} \cdot \ln(e) \quad (7)$$

where:

- λ is the center band wavelength of the emitted radiance;
- $T_b$ has been calculated using Equation (6);
- e – the emissivity calculated using the Equation (8):

$$e = 0.004 \cdot Pv + 0.986 \quad (8)$$

where Pv is the vegetation rate calculated according to the Equation (9):

$$Pv = \left( \frac{NDVI - NDVI_{min}}{NDVI_{max} - NDVI_{min}} \right)^2 \quad (9)$$

### 2.6. Regression Analysis

Regression equations were calculated for the years 1994, 2009, and 2024. The entirety of NDVI and LST pixels was incorporated into the regression analysis, with NDVI serving as the independent variable and LST as the dependent variable [43, 55]. This choice was made based on the established relationship between vegetation index and LST. The correlation coefficient values generated by the regression analysis using Microsoft Excel 2016 ranged from -1 to +1 [7, 55]. A negative correlation between LST and NDVI was observed in the majority of the studies.

## 3. Results and Discussion

### 3.1. Forest Cover Change Analysis

The classification of satellite images allowed for the identification of five distinct cover types: dense forests, sparse forests, non-forests, cropland, and water bodies. NDVI thresholds were used to classify these types, with dense forests defined by values >0.49, sparse forests ranging from 0.33 to 0.49, and croplands falling below 0.33. The classification results for the years 1994, 2009, and 2024 are depicted in Figure 4 and Table 2.

Table 2

*Land use and land cover classification and change results from 1994 to 2024*

| Classes | Area 1994 | | Area 2009 | | Area 2024 | | Area change 1994-2024 | |
|---|---|---|---|---|---|---|---|---|
| | [km$^2$] | [%] | [km$^2$] | [%] | [km$^2$] | [%] | [km$^2$] | [%] |
| Dense forests | 7,906.99 | 76.62 | 6,660.42 | 64.54 | 6,004.51 | 58.18 | -1,902.48 | -18.43 |
| Sparse forests | 1,722.57 | 16.69 | 2,494.59 | 24.17 | 2,534.48 | 24.56 | 811.91 | 7.87 |
| Non-forests | 329.96 | 3.20 | 45.84 | 0.44 | 70.12 | 0.68 | -259.84 | -2.52 |
| Cropland | 326.09 | 3.16 | 1,075.34 | 10.42 | 1,497.15 | 14.51 | 1,171.06 | 11.35 |
| Water bodies | 34.39 | 0.33 | 43.81 | 0.42 | 213.74 | 2.07 | 179.35 | 1.74 |
| Total | 10,320.00 | 100.00 | 10,320.00 | 100.00 | 10,320.00 | 100.00 | | |

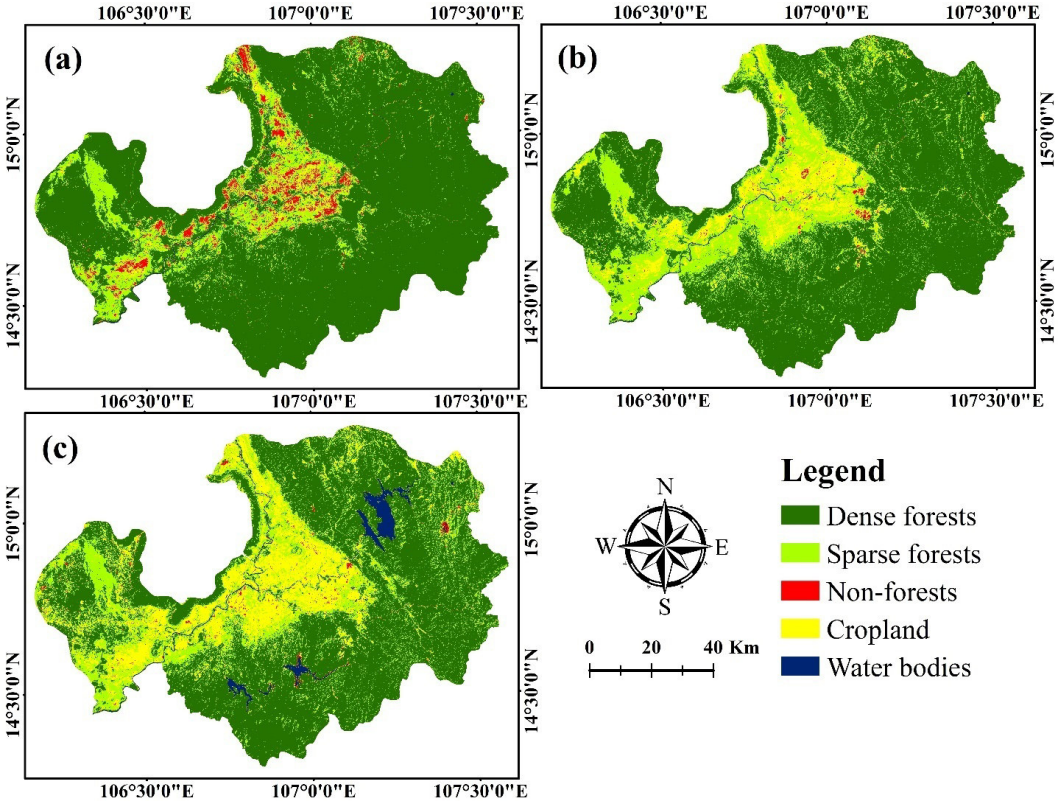


Fig. 4. *Supervised classification results using maximum likelihood classification algorithm in Attapeu province, Lao PDR: a. 1994; b. 2009; c. 2024*

The post-classification results were also evaluated for accuracy using error matrices, resulting in overall accuracies of 92.67, 93.67, and 95.00% for the years 1994, 2009, and 2024, respectively. Additionally, the kappa coefficient was applied to assess the level of agreement between the classification results and the ground reference data. The kappa coefficients were determined to be 0.891 for 1994, 0.902 for 2009, and 0.929 for 2024. The results obtained from calculating the overall accuracy and kappa coefficients indicate high consistency between the classified maps and the reference data. The trends observed in Attapeu province are consistent with findings from Thailand, where dense forest cover declined by 5% over 15 years due to expanding agricultural land [18].

Our findings demonstrate a significant decrease in dense forests, from 7,906.99 $km^2$ (76.62%) in 1994 to 6,660.42 $km^2$ (64.54%) in 2009, further decreasing to 6,004.51 $km^2$ (58.18%) by 2024. This implies a loss of 1,902.48 $km^2$ (18.43%) in Attapeu province. The area of sparse forests shows a positive trend, increasing from 1,722.57 $km^2$ (16.69%) in 1994 to 2,534.48 $km^2$ (24.56%) in 2024, with a net increase of 811.91 $km^2$(7.87%). The area of non-forests decreased from 329.96 $km^2$ (3.20%) in 1994 to 45.84 $km^2$ (0.44%) in 2009, then increased to 70.12 $km^2$ (0.68%) in 2024. However, over the 30-year period (1994-2024), the area of non-forests

decreased by 259.84 $km^2$ (2.52%). Meanwhile, cropland and water bodies have continuously increased from 1994 to 2024, with total increases of 1,171.06 $km^2$ (11.35%) and 179.35 $km^2$ (1.74%), respectively (Table 3). Overall, over the past 30 years, cover types have experienced significant fluctuations in area due to various factors [33, 55]. These factors include human impact, forest encroachment for agriculture, wildfires, unsustainable exploitation of forest resources, illegal logging, shifting cultivation practices, low awareness among the population regarding forest protection, and ineffective state policies and management practices [43, 49]. These factors may lead to forest area reductions, causing severe ecological imbalance, and, more seriously, contributing to global warming [38, 43, 45]. Economic pressures, such as subsistence farming and shifting cultivation, are significant drivers of deforestation in Attapeu. Similar challenges in Vietnam highlight how population growth exacerbates the strain on forest resources [38, 55].

Out of the total area of 7,906.99 $km^2$ of dense forests in 1994, 5,913.06 $km^2$ remained as dense forest in 2024 (Figure 5 and Table 3). However, 1,348.35 $km^2$ were converted to sparse forest, 35.87 $km^2$ to non-forest, and 447.96 $km^2$ to cropland, with the remaining area converted to water bodies (161.75 $km^2$). For the sparse forest class, 1,112.29 $km^2$ out of the initial 1,722.57 $km^2$ in 1994 remained, with the majority of this area converted to cropland (505.05 $km^2$), and the remaining portion converted to dense forest, non-forest, and water bodies (Table 3). The area of non-forest land decreased from 329.96 $km^2$ in 1994 to 70.12 $km^2$ in 2024, with most of this area converted to cropland (311.44 $km^2$), and only 11.76 $km^2$ remaining unchanged or converted to other land cover classes. Meanwhile, the initial cropland area was only 326.09 $km^2$ in 1994, but over the 30-year period, it received the most area from other land cover classes, increasing to 1,497.15 $km^2$ by 2024 (Table 3). Additionally, the area of water bodies also increased from 34.39 $km^2$ in 1994 to 213.74 $km^2$, primarily due to the conversion of dense forest, as mentioned above.

Table 3

Cross-tabulation of land cover classes between 1994 and 2024 (area in $km^2$)

| 1994 / 2024 | Dense forests | Sparse forests | Non-forests | Cropland | Water bodies | Total (2024) |
|---|---|---|---|---|---|---|
| Dense forests | 5,913.06 | 80.25 | 4.13 | 7.07 | 0 | 6004.51 |
| Sparse forests | 1,348.35 | 1,112.29 | 18.46 | 55.38 | 0 | 2,534.48 |
| Non-forests | 35.87 | 14.85 | 11.76 | 6.39 | 1.25 | 70.12 |
| Cropland | 447.96 | 505.05 | 286.99 | 255.26 | 1.89 | 1,497.15 |
| Water bodies | 161.75 | 10.13 | 8.62 | 1.99 | 31.25 | 213.74 |
| Total (1994) | 7,906.99 | 1,722.57 | 329.96 | 326.09 | 34.39 | |

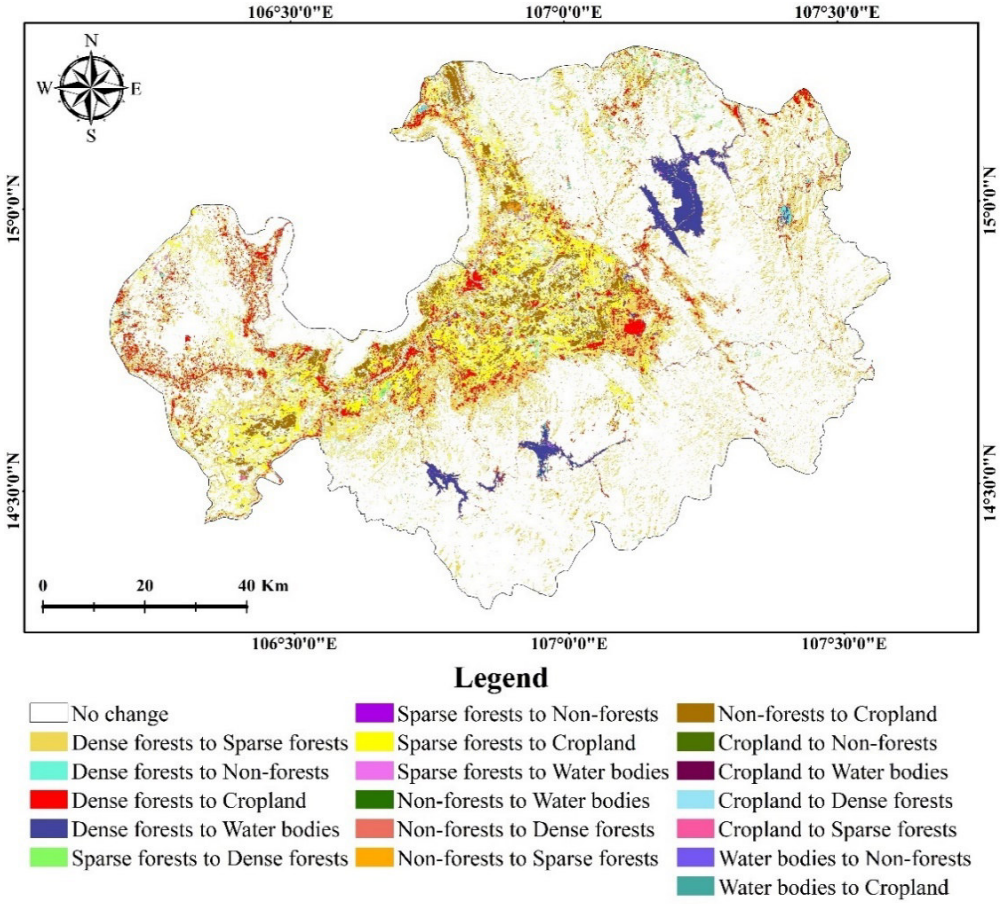


Fig. 5. *Land use and land cover changes map in Attapeu province from 1994 to 2024*

The current study focuses on changes in forest cover in Attapeu province and has found a decrease of 1,902.48 $km^2$ (18.43%) in dense forests area from 1994 to 2024. Meanwhile, there has been an increase of 845.19 $km^2$ (8.19%) in sparse forests area during the same period. The deforestation in Attapeu province, Lao PDR, is causing serious impacts on the environment and the livelihoods of the community [47, 62]. The main causes of this situation include unsustainable logging, land development to meet economic and social demands, along with forest fires [38, 48]. The consequences of deforestation are not limited to the loss of timber supply and wildlife habitats but also affect soil temperature. Deforestation reduces the ability to absorb solar energy and increases soil temperature [17, 35]. Additionally, deforestation leads to natural soil erosion and increases the risk of landslides, posing serious problems for infrastructure and the lives of local people [15, 32]. This study also indicates that the continuous expansion of cropland over the past 30 years has contributed to the conversion of dense forests into sparse forests. Lao PDR is a developing country with its economy heavily reliant on agriculture, but agricultural techniques and practices remain limited, leading to

ongoing deforestation for shifting cultivation [26, 60]. Furthermore, the study area harbors many rare and valuable timber species, leading to illegal logging and further shrinking of forested areas. This calls for attention and action from government agencies, non-governmental organizations, and the community to protect and restore these valuable forest areas, ensuring a balance between economic development and environmental conservation [31, 55, 60].

### 3.2. LST Variation in Attapeu Province from 1994 to 2024

The results of LST for the three datasets of TIRS, namely 1994, 2009, and 2024, as well as spatial and temporal changes arediscussed (Figure 6).

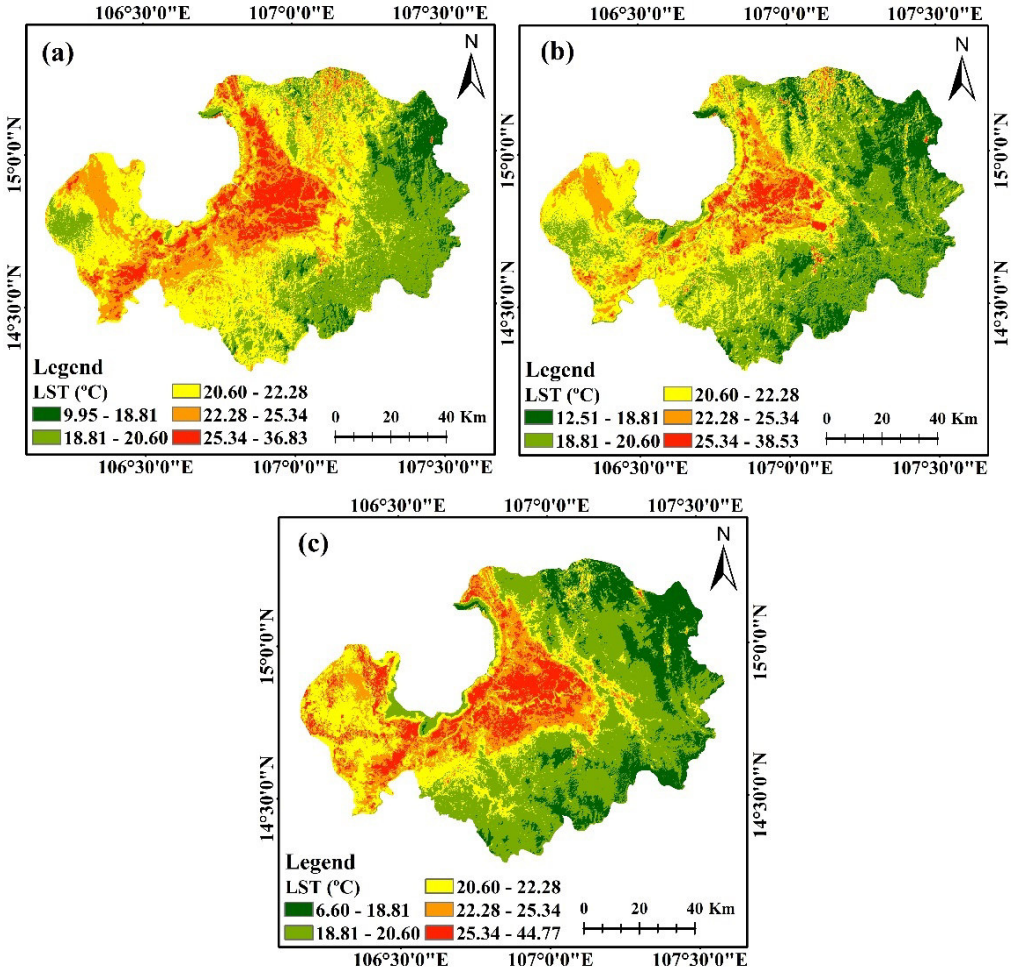


Fig. 6. *Spatial distribution of LST in: a. 1994; b. 2009; c. 2024*

According to the statistics, for the years 1994, 2009, and 2024, the research area was divided into three groups of LST: low temperature, moderate temperature, and high temperature [43]. Low temperatures mainly occurred in dense forests and

water bodies, moderate temperatures in sparse forests, and high temperatures in non-forest areas and cropland. The LST retrieval results indicate a decreasing trend in temperature for sparse forests and increasing temperature for the remaining four land cover types: dense forests, non-forest, cropland, and water bodies from 1994 to 2009. However, from 2009 to 2024, these values have significantly decreased for all land cover types. This decrease may be attributed to localized reforestation initiatives and climate patterns, such as enhanced rainfall variability during this period [59, 61]. The amplitude of LST fluctuations gradually increases from 1994 to 2024. The observed phenomena could be attributed to the reduction in dense forest cover and the expansion of non-forest and cropland areas. Furthermore, the pronounced and recent fluctuations in LST seem to be closely linked to global warming. Consequently, the redistribution of moisture across different regions may exert control over global temperature patterns.

The spatial distribution of LST across various forest cover types was assessed using the TIRS dataset from Landsat.Sparse forests exhibited lower LST trends compared to croplands, likely due to partial canopy cover allowing for moderate evapotranspiration, which reduces heat absorption by the soil [10, 22]. LST trends were found to correspond with different types of forest cover and land use, indicating lower temperatures in dense forests, sparse forests, and water bodies, whereas higher temperatures were observed in non-forest areas and croplands. The estimation of LST utilizing TIRS involved calculating the radiant energy emitted from diverse ground surface types, including paved areas, bare soil, vegetation canopy, and regions affected by water pressure [13, 37, 43]. For this study, three representative years were chosen to illustrate LST values across forest cover types, as depicted in Table 4 and Figure 7.

Table 4

*Range and mean values of LST (°C) for different LULC types in 1994, 2009, and 2024*

| Classes | LST in 1994 | | LST in 2009 | | LST in 2024 | |
|---|---|---|---|---|---|---|
| | Range | Mean ± std. dev. | Range | Mean ± std. dev. | Range | Mean ± std. dev. |
| Dense forests | 12.36 – 32.46 | 20.59 ± 1.40 | 15.79 – 32.20 | 21.83 ± 0.98 | 8.62 – 43.48 | 17.00 ± 1.73 |
| Sparse forests | 10.93 – 35.26 | 23.93 ± 1.82 | 15.33 – 35.41 | 23.21 ± 1.70 | 8.03 – 44.77 | 19.38 ± 2.90 |
| Non-forests | 9.96 – 36.83 | 27.15 ± 2.20 | 12.98 –3 8.54 | 28.15 ± 3.64 | 6.60 – 39.44 | 22.13 ± 3.93 |
| Cropland | 10.93 – 36.05 | 26.01 ± 1.92 | 13.93 – 38.15 | 26.41 ± 2.05 | 6.70 – 42.44 | 22.60 ± 2.56 |
| Water bodies | 9.95 – 33.66 | 21.65 ± 1.45 | 12.51 – 35.80 | 22.29 ± 2.02 | 11.67 – 28.92 | 17.63 ± 1.09 |

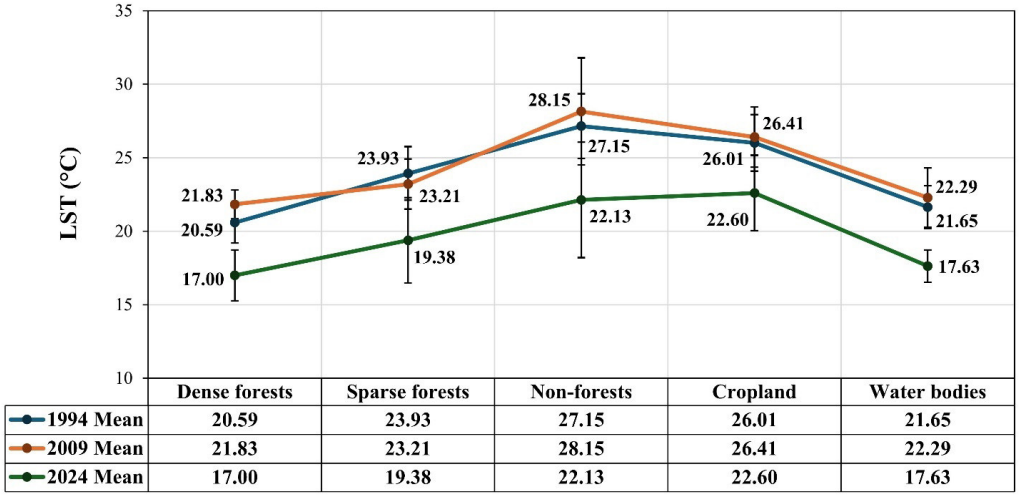


| | Dense forests | Sparse forests | Non-forests | Cropland | Water bodies |
|---|---|---|---|---|---|
| 1994 Mean | 20.59 | 23.93 | 27.15 | 26.01 | 21.65 |
| 2009 Mean | 21.83 | 23.21 | 28.15 | 26.41 | 22.29 |
| 2024 Mean | 17.00 | 19.38 | 22.13 | 22.60 | 17.63 |

Fig. 7. *Mean LST change over several land use and land cover types in 1994, 2009, and 2024*

The statistical analysis of LST for various land cover types in the years 1994, 2009, and 2024 revealed fluctuations ranging from the lowest to the highest values. From 1994 to 2009, the mean values of dense forests, non-forest, cropland, and water bodies increased from 20.59 to 21.83°C, 27.15 to 28.15°C, 26.01 to 26.41°C, and 21.65 to 22.29°C, respectively, whereas only sparse forest had a decreased average value from 23.93 (1994) to 23.21°C (2009). By 2024, the mean values of all these classes have decreased to 17.00°C (dense forests), 19.38°C (sparse forests), 22.13°C (non-forests), 22.60°C (cropland), and 17.63°C (water bodies). In 2024, despite the significant fluctuations in LST within land cover types, the mean values have been much lower compared to the two previous years (1994 and 2009). The period under observation showed the highest average LST in non-forest areas and croplands, whereas areas covered by dense forests and water bodies exhibited the lowest average LST during the same timeframe. This decrease in LST can be attributed to the enhanced absorption of solar radiation by vegetation [27, 44]. Notably, the average radiative LST of forest canopies, encompassing both dense and sparse forests, was significantly lower during this period. This phenomenon arises from the evapotranspiration process, which reduces the amount of heat retained by natural vegetation cover, coupled with reduced exposure of soil and denser forest canopy [6, 43, 61].

### 3.3. NDVI Variation in Attapeu Province from 1994 to 2024

NDVI offers crucial insights into the spatial distribution, intensity, and continuity of organic vegetation, playing a pivotal role in modulating the variation of LST. Figure 8 illustrates the spatial distribution and vegetation patterns as highlighted by the NDVI values. We observe that non-forest areas and water bodies range from light blue to dark blue, croplands appear white, while sparse

forests and dense forests range from light green to dark green. The estimated NDVI values fluctuate from -0.42 to 0.78 for the year 1994, -0.42 to 0.77 for 2009, and -0.33 to 0.62 for 2024. The results indicate a continuous decrease in NDVI values from 1994 to 2024, suggesting a decline in vegetation cover over the specified period in water bodies and non-forested central areas. Some regional factors are believed to correspond to LST conditions, such as vegetation density, grazing, fuel, and livestock feed [22, 24, 29]. Factors driving temperature increase, such as artificial activities, originate at the local level [27, 55].

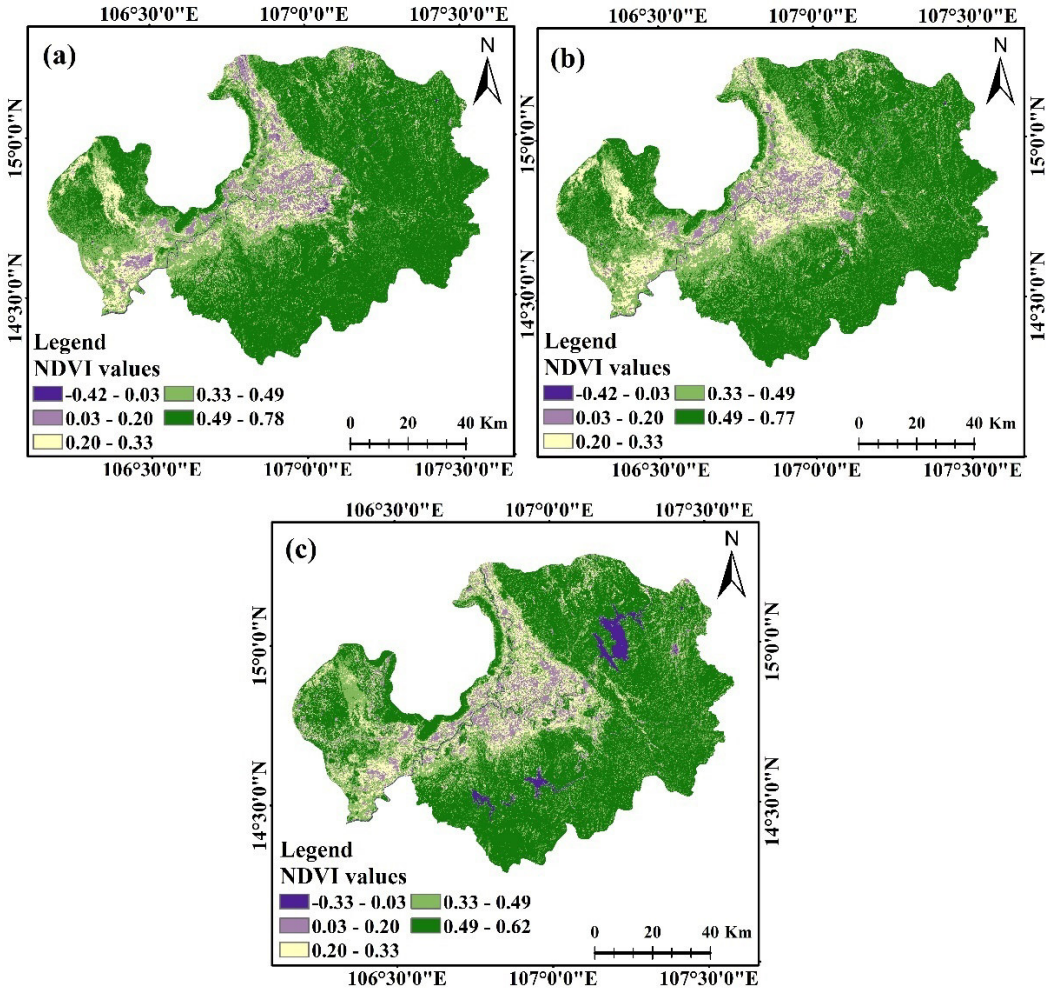


Fig. 8. *Spatial distribution of NDVI in: a. 1994; b. 2009; c. 2024*

### 3.4. Relationship between LST and NDVI

In Attapeu province, the local climatic conditions are intricately linked to the presence of vegetation cover. The alteration of forest cover is closely associated with the expansion of croplands and changes in surface vegetation conditions. The interplay between LST and climate change exhibits

a nuanced relationship with fluctuations in forest cover area. The correlation between NDVI and LST reveals a consistent pattern: as forest cover increases, LST tends to decrease.The weakening correlation between NDVI and LST suggests that intensified human activities and climatic shifts, such as extended droughts, have diminished the cooling effect of vegetation cover [13, 14]. This inverse relationship is evident in our study, with $R^2$ values of 0.5896 in 1994, 0.5691 in 2009, and 0.4344 in 2024, accompanied by corresponding R values of -0.7679, -0.7544, and -0.6591, respectively (Figure 9). The observed inverse correlation between LST and NDVI supports the notion of reduced biomass or vegetation cover in the research area. Areas with higher NDVI values indicate ample vegetation cover capable of exerting a cooling effect by lowering surface temperatures [29, 45]. Through processes such as evapotranspiration and photosynthesis, vegetation plays a crucial role in temperature regulation by absorbing solar energy and enhancing soil moisture and surface permeability [2, 22, 43].

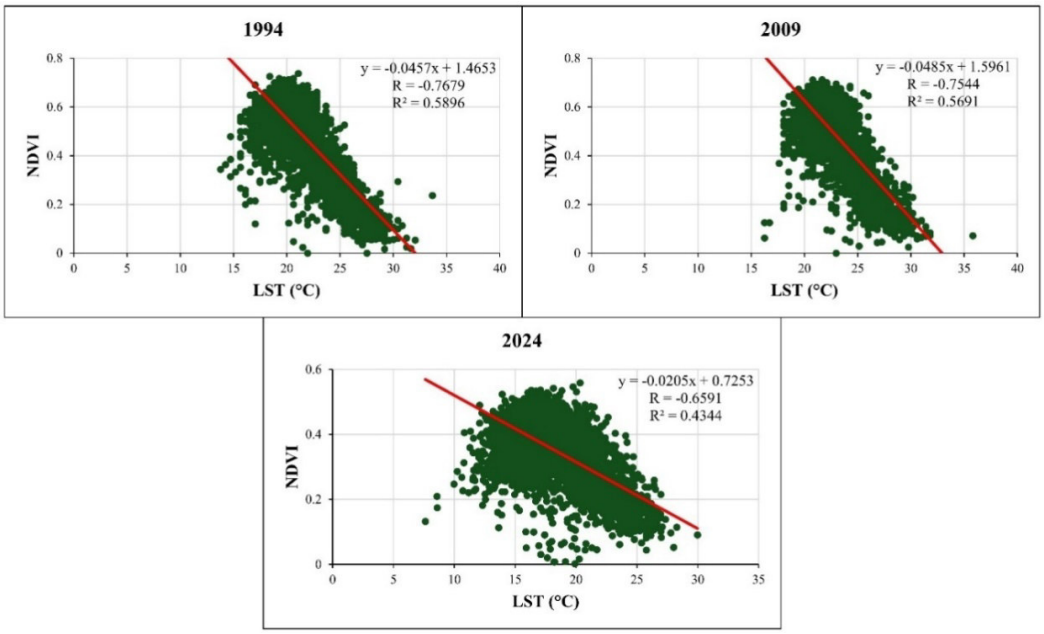


Fig. 9. *Linear regression models between NDVI and LST in 1994, 2009, and 2024*

## 4. Conclusions

In this study, a multi-temporal analysis of Landsat data from 1994 to 2024 was conducted, in order to examine changes in forest cover and LST in Attapeu province, Lao PDR. The analysis revealed that dense forests predominated over the surveyed area, with a notable decrease of 18.43% in dense forest cover and a corresponding increase of 7.47% in sparse forest cover during the period 1994-2024, attributable to both human activities and natural factors. The fluctuation in LST ranged from 9.95 to 36.83°C in 1994, 12.51 to 38.53°C in 2009, and 6.60 to 44.77°C in 2024.

Higher LST values were consistently observed in non-forest and cropland areas, while areas with forest cover and water bodies exhibited lower LST values. The study also observed an inverse correlation between NDVI and LST, with $R^2$ values decreasing over time (from 0.5896 in 1994 to 0.4344 in 2024), indicating a weakening relationship between vegetation cover and surface temperature. Importantly, the study suggests that global warming is the primary driver of recent and intense LST fluctuations rather than changes in land cover classes.

These findings underscore the urgent need for specific conservation measures in the study area. Recommendations for forest conservation include strengthening enforcement against illegal logging, which has contributed to the reduction in dense forest areas, and encouraging agroforestry practices to reduce the expansion of cropland into forested areas. The study highlights the importance of understanding forest and highland ecosystems for effective species conservation and community engagement. By offering data on the temporal dynamics of forest cover and LST, this study can help inform provincial policies and conservation programs, particularly in integrating climate change adaptation strategies into land-use planning. Implementing successful reforestation initiatives, combined with strict law enforcement and agroforestry adoption, is essential for mitigating forest degradation and ensuring ecosystem resilience in Attapeu province.

**References**

1. Adam, E., Mutanga, O., Odindi, J. et al., 2014. Land-use/cover classification in a heterogeneous coastal landscape using RapidEye imagery: evaluating the performance of random forest and support vector machines classifiers. In: International Journal of Remote Sensing, vol. 35(10), pp. 3440-3458. DOI: 10.1080/01431161.2014.903435.
2. Alademomi, A.S., Okolie, C.J., Daramola, O.E. et al., 2022. The interrelationship between LST, NDVI, NDBI, and land cover change in a section of Lagos metropolis, Nigeria. In: Applied Geomatics, vol. 14(2), pp. 299-314. DOI: 10.1007/s12518-022-00434-2.
3. Angessa, A.T., Lemma, B., Yeshitela, K., 2021. Land-use and land-cover dynamics and their drivers in the central highlands of Ethiopia with special reference to the Lake Wanchi watershed. In: GeoJournal, vol. 86(3), pp. 1225-1243. DOI: 10.1007/s10708-019-10130-1.
4. Balew, A., Korme, T., 2020. Monitoring land surface temperature in Bahir Dar city and its surrounding using Landsat images. In: The Egyptian Journal of Remote Sensing and Space Science, vol. 23(3), pp. 371-386. DOI: 10.1016/j.ejrs.2020.02.001.
5. Balha, A., Mallick, J., Pandey, S. et al., 2021. A comparative analysis of different pixel and object-based classification algorithms using multi-source high spatial resolution satellite data for LULC mapping. In: Earth Science Informatics, vol. 14(4), pp. 2231-2247. DOI: 10.1007/s12145-

021-00685-4.
6. Berg, A., Sheffield, J., 2018. Climate change and drought: the soil moisture perspective. In: Current Climate Change Reports, vol. 4(2), pp. 180-191. DOI: 10.1007/s40641-018-0095-0.
7. Busico, G., Kazakis, N., Cuoco, E. et al., 2020. A novel hybrid method of specific vulnerability to anthropogenic pollution using multivariate statistical and regression analyses. In: Water Research, vol. 171, ID article 115386. DOI: 10.1016/j.watres.2019.115386.
8. Chicco, D., Warrens, M.J., Jurman, G., 2021. The Matthews correlation coefficient (MCC) is more informative than Cohen's Kappa and Brier score in binary classification assessment. In: IEEE Access, vol. 9, pp. 78368-78381. DOI: 10.1109/ACCESS.2021.3084050.
9. Choudhury, D., Das, K., Das, A., 2019. Assessment of land use land cover changes and its impact on variations of land surface temperature in Asansol-Durgapur Development Region. In: The Egyptian Journal of Remote Sensing and Space Science, vol. 22(2), pp. 203-218. DOI: 10.1016/j.ejrs.2018.05.004.
10. Du, Z., Yu, L., Yang, J. et al., 2023. Mapping annual global forest gain from 1983 to 2021 with landsat imagery. In: IEEE – Journal of Selected Topics in Applied Earth Observations and Remote Sensing, vol. 16, pp. 4195-4204. DOI: 10.1109/JSTARS.2023.3267796.
11. Duan, X., Chen, Y., Wang, L. et al., 2023. The impact of land use and land cover changes on the landscape pattern and ecosystem service value in Sanjiangyuan region of the Qinghai-Tibet Plateau. In: Journal of Environmental Management, vol. 325, Part B, ID article 116539. DOI: 10.1016/j.jenvman.2022.116539.
12. Getachew, B., Manjunatha, B.R., Bhat, H.G., 2021. Modeling projected impacts of climate and land use/land cover changes on hydrological responses in the Lake Tana Basin, upper Blue Nile River Basin, Ethiopia. In: Journal of Hydrology, vol. 595, ID article 125974. DOI: 10.1016/j.jhydrol.2021.125974.
13. Gohain, K.J., Mohammad, P., Goswami, A., 2021. Assessing the impact of land use land cover changes on land surface temperature over Pune city, India. In: Quaternary International, vol. 575, pp. 259-269. DOI: 10.1016/j.quaint.2020.04.052.
14. Guha, S., Govil, H., Dey, A. et al., 2018. Analytical study of land surface temperature with NDVI and NDBI using Landsat 8 OLI and TIRS data in Florence and Naples city, Italy. In: European Journal of Remote Sensing, vol. 51(1), pp. 667-678. DOI: 10.1080/22797254.2018.1474494.
15. Haldar, S., Mandal, S., Bhattacharya, S. et al., 2023. Dynamicity of land use/land cover (LULC): An analysis from peri-urban and rural neighbourhoods of Durgapur Municipal Corporation (DMC) in India. In: Regional Sustainability, vol. 4(2), pp. 150-172. DOI: 10.1016/j.regsus.2023.05.001.
16. Hao, Y., Liu, S., Lu, Z.N. et al., 2018. The impact of environmental pollution on public health expenditure: dynamic panel analysis based on Chinese provincial data. In: Environmental Science and Pollution Research, vol. 25(19), pp. 18853-

18865. DOI: 10.1007/s11356-018-2095-y.
17. He, P., Baiocchi, G., Hubacek, K. et al., 2018. The environmental impacts of rapidly changing diets and their nutritional quality in China. In: Nature Sustainability, vol. 1(3), pp. 122-127. DOI: 10.1038/s41893-018-0035-y.
18. Hermhuk, S., Chaiyes, A., Thinkampheang, S. et al., 2020. Land use and above-ground biomass changes in a mountain ecosystem, northern Thailand. In: Journal of Forestry Research, vol. 31, pp. 1733-1742. DOI:10.1007/s11676-019-00924-x.
19. Hua, A.K., Ping, O.W., 2018. The influence of land-use/land-cover changes on land surface temperature: a case study of Kuala Lumpur metropolitan city. In: European Journal of Remote Sensing, vol. 51(1), pp. 1049-1069. DOI: 10.1080/22797254.2018.1542976.
20. Hussain, S., Mubeen, M., Ahmad, A. et al., 2022. Assessment of land use/land cover changes and its effect on land surface temperature using remote sensing techniques in Southern Punjab, Pakistan. In: Environmental Science and Pollution Research, vol. 30(44), pp. 99202-99218. DOI: 10.1007/s11356-022-21650-8.
21. Ilunga, A., 2024. Impact of climate change on plant diversity in tropical rainforests. In: American Journal of Natural Sciences, vol. 5(2), pp. 1-10. DOI: 10.47672/ajns.2041.
22. Kafy, A.A., Al Rakib, A., Fattah, M.A. et al., 2022. Impact of vegetation cover loss on surface temperature and carbon emission in a fastest-growing city, Cumilla, Bangladesh. In: Building and Environment, vol. 208, ID article 108573. DOI: 10.1016/j.buildenv.2021.108573.
23. Kafy, A.A., Dey, N.N., Al Rakib, A. et al., 2021. Modeling the relationship between land use/land cover and land surface temperature in Dhaka, Bangladesh using CA-ANN algorithm. In: Environmental Challenges, vol. 4, ID article 100190. DOI: 10.1016/j.envc.2021.100190.
24. Kafy, A.A., Rahman, M.S., Hasan, M.M. et al., 2020. Modelling future land use land cover changes and their impacts on land surface temperatures in Rajshahi, Bangladesh. In: Remote Sensing Applications: Society and Environment, vol. 18, ID article 100314. DOI: 10.1016/j.rsase.2020.100314.
25. Khandelwal, S., Goyal, R., Kaul, N. et al., 2018. Assessment of land surface temperature variation due to change in elevation of area surrounding Jaipur, India. In: The Egyptian Journal of Remote Sensing and Space Science, vol. 21(1), pp. 87-94. DOI: 10.1016/j.ejrs.2017.01.005.
26. Leta, M.K., Demissie, T.A., Tränckner, J., 2021. Modeling and prediction of land use land cover change dynamics based on land change modeler (Lcm) in nashe watershed, upper blue nile basin, Ethiopia. In: Sustainability, vol. 13(7), ID article 3740. DOI: 10.3390/su13073740.
27. Mathew, A., Sarwesh, P., Khandelwal, S., 2022. Investigating the contrast diurnal relationship of land surface temperatures with various surface parameters represent vegetation, soil, water, and urbanization over Ahmedabad city in India. In: Energy Nexus, vol. 5, ID article 100044. DOI:

10.1016/j.nexus.2022.100044.

28. Mehmood, M.S., Rehman, A., Sajjad, M. et al., 2023. Evaluating land use/cover change associations with urban surface temperature via machine learning and spatial modeling: Past trends and future simulations in Dera Ghazi Khan, Pakistan. In: Frontiers in Ecology and Evolution, vol. 11, ID article 1115074. DOI: 10.3389/fevo.2023.1115074.
29. Moazzam, M.F.U., Doh, Y.H., Lee, B.G., 2022. Impact of urbanization on land surface temperature and surface urban heat Island using optical remote sensing data: A case study of Jeju Island, Republic of Korea. In: Building and Environment, vol. 222, ID article 109368. DOI: 10.1016/j.buildenv.2022.109368.
30. Moisa, M.B., Dejene, I.N., Gemeda, D.O., 2022. Integration of geospatial technologies with multiple regression model for urban land use land cover change analysis and its impact on land surface temperature in Jimma City, southwestern Ethiopia. In: Applied Geomatics, vol. 14(4), pp. 653-667. DOI: 10.1007/s12518-022-00463-x.
31. Moser-Reischl, A., Uhl, E., Rötzer, T. et al., 2018. Effects of the urban heat island and climate change on the growth of Khaya senegalensis in Hanoi, Vietnam. In: Forest Ecosystems, vol. 5(1), ID artilce 37. DOI: 10.1186/s40663-018-0155-x.
32. Nguyen, T.M., Lin, T.H., Chan, H.P., 2019. The environmental effects of urban development in Hanoi, Vietnam from satellite and meteorological observations from 1999–2016. In: Sustainability, vol. 11(6), ID article 1768. DOI: 10.3390/su11061768.
33. Obeidat, M., Awawdeh, M., Lababneh, A., 2019. Assessment of land use/land cover change and its environmental impacts using remote sensing and GIS techniques, Yarmouk River Basin, north Jordan. In: Arabian Journal of Geosciences, vol. 12(22), ID article 685. DOI: 10.1007/s12517-019-4905-z.
34. Office of the Governor of Attapeu Province, 2023. History, special points and potential. Available at: https://www.attapeu.gov.la/en/abouttprovince/informatoin-pro/.html. Accessed on: January 10, 2024.
35. Ogato, G.S., Bantider, A., Abebe, K. et al., 2020. Geographic information system (GIS)-based multicriteria analysis of flooding hazard and risk in Ambo Town and its watershed, West shoa zone, oromia regional State, Ethiopia. In: Journal of Hydrology: Regional Studies, vol. 27, ID article 100659. DOI: 10.1016/j.ejrh.2019.100659.
36. Orimoloye, I.R., Olusola, A.O., Belle, J.A. et al., 2022. Drought disaster monitoring and land use dynamics: identification of drought drivers using regression-based algorithms. In: Natural Hazards, vol. 112(2), pp. 1085-1106. DOI: 10.1007/s11069-022-05219-9.
37. Peng, J., Ma, J., Liu, Q. et al., 2018. Spatial-temporal change of land surface temperature across 285 cities in China: An urban-rural contrast perspective. In: Science of The Total Environment, vol. 635, pp. 487-497. DOI: 10.1016/j.scitotenv.2018.04.105.
38. Phuong, V.T., Thien, B.B., 2023. Using Landsat satellite images to detect

forest cover changes in the Northeast region of Vietnam. In: Bulletin of the Transilvania University of Brasov, Series II: Forestry, Wood Industry, Agricultural Food Engineering, vol. 16(1), pp. 19-36. DOI: 10.31926/but.fwiafe.2023.16.65.1.2.

39. Phuong, V.T., Thien, B.B., 2024. Land use change mapping and analysis using remote sensing and GIS: A case study in Tam Ky City, Quang Nam Province, Vietnam. In: Journal of Multidisciplinary Applied Natural Science, vol. 4(2), pp. 210-224. DOI: 10.5775/fg.2023.030.i.
40. Pullanikkatil, D., Palamuleni, L.G., Ruhiiga, T.M., 2016. Land use/land cover change and implications for ecosystems services in the Likangala River Catchment, Malawi. In: Physics and Chemistry of the Earth, Parts A/B/C, vol. 93, pp. 96-103. DOI: 10.1016/j.pce.2016.03.002.
41. Qiao, Z., Liu, L., Qin, Y. et al., 2020. The impact of urban renewal on land surface temperature changes: A case study in the main city of Guangzhou, China. In: Remote Sensing, vol. 12(5), ID article 794. DOI: 10.3390/rs12050794.
42. Rahman, M.U., Dey, T., Biswas, J., 2023. Land-use change and forest cover depletion in Bhawal National Park, Gazipur, Bangladesh from 2005 to 2020. In: Environmental Monitoring and Assessment, vol. 195(1), ID article 201. DOI: 10.1007/s10661-022-10764-8.
43. Raihan, A., Tuspekova, A., 2022. Dynamic impacts of economic growth, energy use, urbanization, tourism, agricultural value-added, and forested area on carbon dioxide emissions in Brazil. In: Journal of Environmental Studies and Sciences, vol. 12(4), pp. 794-814. DOI: 10.1007/s13412-022-00782-w.
44. Sekertekin, A., Bonafoni, S., 2020. Land surface temperature retrieval from Landsat 5, 7, and 8 over rural areas: Assessment of different retrieval algorithms and emissivity models and toolbox implementation. In: Remote Sensing, vol. 12(2), ID article 294. DOI: 10.3390/rs12020294.
45. Sekertekin, A., Zadbagher, E., 2021. Simulation of future land surface temperature distribution and evaluating surface urban heat island based on impervious surface area. In: Ecological Indicators, vol. 122, ID article 107230. DOI: 10.1016/j.ecolind.2020.107230.
46. Shiraishi, T., Motohka, T., Thapa, R.B. et al., 2014. Comparative assessment of supervised classifiers for land use–land cover classification in a tropical region using time-series PALSAR mosaic data. In: IEEE - Journal of Selected Topics in Applied Earth Observations and Remote Sensing, vol. 7(4), pp. 1186-1199. DOI: 10.1109/JSTARS.2014.2313572.
47. Sohail, M.T., Mahfooz, Y., Azam, K. et al., 2019. Impacts of urbanization and land cover dynamics on underground water in Islamabad, Pakistan. In: Desalination and Water Treatment, vol. 159, pp. 402-411. DOI: 10.5004/dwt.2019.24156.
48. Statuto, D., Cillis, G., Picuno, P., 2019. GIS-based analysis of temporal evolution of rural landscape: A case study in Southern Italy. In: Natural Resources Research, vol. 28(S1), pp. 61-75. DOI: 10.1007/s11053-018-9402-7.

49. Tan, J., Yu, D., Li, Q. et al., 2020. Spatial relationship between land-use/land-cover change and land surface temperature in the Dongting Lake area, China. In: Scientific Reports, vol. 10(1), ID article 9245. DOI: 10.1038/s41598-020-66168-6.
50. Tariq, A., Shu, H., 2020. CA-Markov chain analysis of seasonal land surface temperature and land use land cover change using optical multi-temporal satellite data of Faisalabad, Pakistan. In: Remote Sensing, vol. 12(20), ID article 3402. DOI: 10.3390/rs12203402.
51. Thakur, P.K., Samant, S.S., Verma, R.K. et al., 2024. Monitoring forest cover changes and its impact on land surface temperature using geospatial technique in Talra Wildlife Sanctuary, Shimla, India. In: Environment, Development and Sustainability, pp. 1-30. DOI: 10.1007/s10668-023-04347-x
52. Thakur, S., Maity, D., Mondal, I. et al., 2021. Assessment of changes in land use, land cover, and land surface temperature in the mangrove forest of Sundarbans, northeast coast of India. In: Environment, Development and Sustainability, vol. 23(2), pp. 1917-1943. DOI: 10.1007/s10668-020-00656-7.
53. Thien, B.B., Ovsepyan, A.E., Phuong, V.T., 2024. Monitoring land surface temperature relationship to land use and land cover in Hai Duong Province, Vietnam. In: Environment and Natural Resources Journal, vol. 22(2), pp. 145-157. DOI: 10.32526/ennrj/22/20230194.
54. Thien, B.B., Phuong, V.T., 2024a. Analyzing and modeling land use/land cover change in Phu Tho Province, Vietnam. In: Journal of Degraded and Mining Lands Management, vol. 11(2), pp. 5225-5235. DOI: 10.15243/jdmlm.2024.112.5225.
55. Thien, B.B., Phuong, V.T., 2024b. Assessing the impact of land use/land cover changes on agricultural land in the Red River Delta, Vietnam. In: Vegetos, vol. 37, pp. 606-617. DOI: 10.1007/s42535-023-00769-0.
56. Ullah, S., Ahmad, K., Sajjad, R.U. et al., 2019. Analysis and simulation of land cover changes and their impacts on land surface temperature in a lower Himalayan region. In: Journal of Environmental Management, vol. 245, pp. 348-357. DOI: 10.1016/j.jenvman.2019.05.063.
57. Vivekananda, G., Swathi, R., Sujith, A., 2021. Multi-temporal image analysis for LULC classification and change detection. In: European Journal of Remote Sensing, vol. 54(sup2), pp. 189-199. DOI: 10.1080/22797254.2020.1771215.
58. Wang, J., Azam, W., 2024. Natural resource scarcity, fossil fuel energy consumption, and total greenhouse gas emissions in top emitting countries. In: Geoscience Frontiers, vol. 15(2), ID article 101757. DOI: 10.1016/j.gsf.2023.101757.
59. Watanabe, S., 2024. Impact of deforestation on regional climate patterns in Japan. In: International Journal of Climatic Studies, vol. 3(1), pp. 37-47. DOI: 10.47604/ijcs.2477.
60. Wei, B., Xie, Y., Jia, X. et al., 2018. Land use/land cover change and it's impacts on diurnal temperature range over the agricultural pastoral ecotone of Northern China. In: Land Degradation and Development, vol. 29(9), pp. 3009-3020. DOI:

10.1002/ldr.3052.
61. Yang, J., Jin, S., Xiao, X. et al., 2019. Local climate zone ventilation and urban land surface temperatures: Towards a performance-based and wind-sensitive planning proposal in megacities. In: Sustainable Cities and Society, vol. 47, ID article 101487. DOI: 10.1016/j.scs.2019.101487.
62. Zahoor, Z., Latif, M.I., Khan, I. et al., 2022. Abundance of natural resources and environmental sustainability: the roles of manufacturing value-added, urbanization, and permanent cropland. In: Environmental Science and Pollution Research, vol. 29(54), pp. 82365-82378. DOI: 10.1007/s11356-022-21545-8.